PHYSICAL REVIEW B **86**, 161416(R) (2012)

Long-distance spin transport in high-mobility graphene on hexagonal boron nitride

P. J. Zomer,[*] M. H. D. Guimarães, N. Tombros, and B. J. van Wees

Physics of Nanodevices, Zernike Institute for Advanced Materials, University of Groningen, Groningen, The Netherlands

(Received 10 September 2012; published 31 October 2012)

We performed spin transport measurements on boron nitride based single layer graphene devices with mobilities up to 40 000 cm^2 V^{-1} s^{-1}. We could observe spin transport over lengths up to 20 μm at room temperature, the largest distance measured so far for graphene. Due to enhanced charge-carrier diffusion, spin relaxation lengths are measured up to 4.5 μm. The relaxation times are similar to values for lower quality SiO_2-based devices, around 200 ps. We find that the relaxation rate is determined in almost equal measures by the Elliott-Yafet and D'Yakonov-Perel mechanisms.

DOI: 10.1103/PhysRevB.86.161416 PACS number(s): 75.76.+j, 72.80.Vp, 72.25.−b, 85.75.Hh

The potential of graphene[1] as an emerging material for spintronics has been established, revealing spin relaxation lengths λ of 2 μm at room temperature.[2] Spins relax over a length $\lambda = \sqrt{D_s \tau_s}$, where D_s is the spin diffusion constant and τ_s is the spin relaxation time. One straightforward way to achieve spin transport over larger distances is to enhance D_s by fabricating high-mobility devices. On the other hand, τ_s is theoretically predicted to range up to hundreds of nanoseconds.[3] However, observations made in recent years by experimentalists[2,4–13] do not match up to the high expectations set by theory. Measurements typically indicate τ_s to be in the 100 ps range, and the discrepancy between theory and experiment and the exact relaxation mechanism remain yet unclear. Some works suggest that spin relaxation is dominated by the Elliott-Yafet (EY) mechanism,[4,11,14] where τ_s is proportional to the momentum relaxation time τ_p and spins lose their information during scattering events. Other efforts indicate that the D'Yakonov-Perel (DP) mechanism is stronger,[3,15,16] where τ_s is inversely proportional to τ_p and spins dephase in between scattering events.

In identifying the limiting factors on spin transport in graphene, the substrate deserves special attention. For charge transport it has already been shown that the standard silicon oxide substrate reduces the mobility of charge carriers considerably.[17] The SiO_2 substrate is expected to also affect the spin relaxation in graphene through its roughness, trapped charges, and surface phonons.[16] One approach to reduce the substrate roughness and screen impurities is to use epitaxial graphene on silicon carbide.[12,18] However, for graphene on the silicon face the presence of localized states is believed to affect spin transport in this system.[13] Alternatively, eliminating the influence of the substrate by suspending the graphene flake yields a three orders of magnitude increase in mobility.[19,20] Suspended spintronic graphene devices have been studied and a lower bound for τ_s of ~200 ps was found.[10] Determination of the actual value was, however, not possible since the presence of local supports for the suspended device appeared to dominate the extraction of τ_s.

Atomically flat hexagonal boron nitride (h-BN) was found to be a much better substrate than SiO_2 for high-quality graphene electronics,[21–23] yielding a two orders of magnitude increase in mobility. In this Rapid Communication we present spin transport measurements on h-BN-based graphene devices, which give access to a higher-mobility regime than explored so far in graphene spin transport, while overcoming SiO_2-related issues such as the roughness and the presence of trapped charges.

Devices are made by transfer of a graphene flake (HOPG grade ZYA) onto a h-BN crystal, typically ~20 nm thick, following a transfer recipe described in detail elsewhere.[23] The h-BN crystals are mechanically cleaved from a commercially available boron nitride powder (Momentive PolarTherm, Grade PT110). Electrical contacts to the graphene flake are made using standard electron beam lithography techniques. We first deposit either aluminum or titanium, in both cases in two steps of 0.4 nm, with an oxidation step after each deposition. Secondly we deposit 65-nm cobalt in order to have spin sensitive contacts. The oxide barrier at the contact interface is required to tackle the conductivity mismatch problem, i.e., to prevent spin relaxation through the contacts. Typically the contact resistance is in the order of ~10 kΩ. The standard recipe for high-quality graphene devices on h-BN requires a final anneal step in Ar/H_2 flow at 330 °C for 8 h. We found that this treatment degrades our Co contacts so that they lose their spin injection and detection properties. Therefore we omitted this step here. Also no other annealing steps have been used, keeping the fabrication process the same as for SiO_2-based devices. Measurements are all done in vacuum (~1×10^{-7} mbar), using standard ac lock-in techniques with currents up to 5 μA.

To characterize our devices we determine the field effect mobility μ of the charge carriers: $\mu = 1/neR_{sq}$. Here e is the electron charge and n is the charge-carrier density. The latter is calculated using $n = \frac{C_g}{e}(V - V_D)$, where V is the applied gate voltage, V_D is the gate voltage at which the charge neutrality point is found, and $C_g \approx 67$ μF m^{-2} is the geometric gate capacitance for 500-nm SiO_2 and 20-nm h-BN. For device 2 shown in Fig. 1(a) we deposited the graphene flake partly on top of h-BN and partly on SiO_2, allowing for a direct comparison between charge-carrier transport for both cases. The obtained values for R_{sq} are presented in Fig. 1(b); the inset shows the calculated mobility. The quality improvement due to the h-BN is directly reflected by the enhanced mobility. The inflection point mobilities at room temperature for the three devices presented here are for 1: 40 000 cm^2 V^{-1} s^{-1}, 2: 21 000 cm^2 V^{-1} s^{-1}, and 3: 14 000 cm^2 V^{-1} s^{-1}. The reduction in full width at half maximum of the Dirac peak indicates smaller fluctuations in charge-carrier density for the

 ©2012 American Physical Society

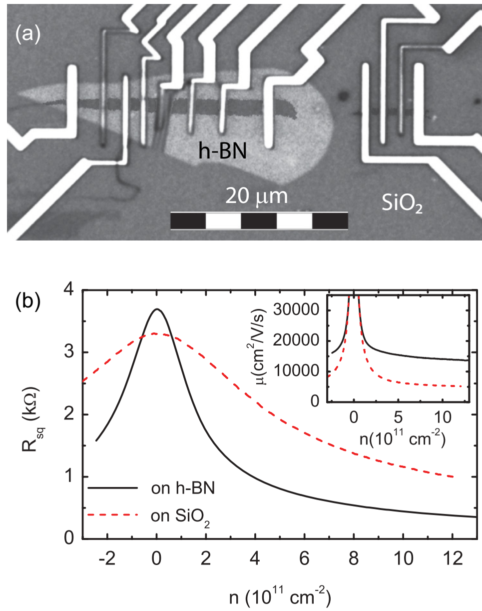

FIG. 1. (Color online) (a) Optical micrograph of device 2, partly on SiO_2 (right side) and partly on h-BN (left side). (b) Square resistance versus charge-carrier density measured on both SiO_2- and h-BN-based parts of the same graphene flake. The inset shows the respective field effect mobilities.

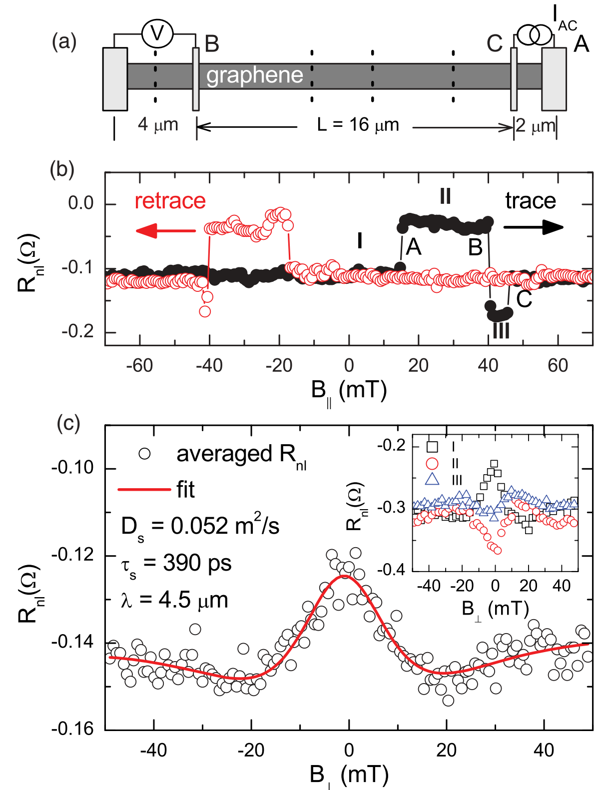

FIG. 2. (Color online) (a) Schematic showing the nonlocal four-terminal geometry for device 3. Contacts not used in the measurement are represented by dashed lines. (b) Spin valve measurement showing the nonlocal resistance versus magnetic field, parallel to the electrodes, at $n = 1.5 \times 10^{12}$ cm^{-2}. Switching of electrodes A to C shows up in the measurement. (c) Hanle spin precession measurement (R_{nl} versus perpendicular magnetic field) averaged between measurements at levels I–III (original data in inset). The solid line shows the fit from which τ_s and D_s are extracted with an error of 16%.

h-BN-supported graphene flake.[19] We find that despite omitting cleaning steps, the charge transport quality is well above that of SiO_2-based graphene spin transport devices.

For spin transport measurements we employ the four-terminal nonlocal technique,[24] schematically shown in Fig. 2(a). We inject a spin-polarized current to the graphene flake by sending an electrical current through the pair of contacts on the right side. The injected spins diffuse through the graphene and arrive at the detection circuit on the left. An external magnetic field applied parallel to the contacts allows for control over their magnetization. Variation in contact width between 130 and 800 nm ensures different coercivity. Spin valve measurements are taken by sweeping the parallel magnetic field while recording the nonlocal resistance R_{nl}, as shown in Fig. 2(b). The switches that occur in one sweep can be traced back to switching the magnetization of a specific contact. What makes this room temperature spin-valve measurement particularly interesting is the large contact spacing. The total length covered is 18 μm, with multiple switches showing up. Note that the largest length over which a spin signal has been observed is 20 μm for this device, which is the largest contact spacing that was available. This is a direct indication of an improved spin relaxation length.

We measure Hanle spin precession by applying an external magnetic field perpendicular to the graphene plane. The diffusing spins will precess at the Larmor frequency $\omega_L = g\mu_B B/\hbar$, where g is the g factor, μ_B is the Bohr magneton, and $\hbar$ is the reduced Planck constant. Figure 2(c) shows one set of precession data. Since in this case contact A contributes strongly to the spin signal, we measure precession for each magnetization geometry (at levels I–III), shown in the inset of Fig. 2(c). Taking all three precession curves into account we can eliminate the contribution of the outer contact. The precession is fit using the one-dimensional Bloch equation in the steady state regime: $D_s \nabla^2 \vec{\mu}_s - \frac{\vec{\mu}_s}{\tau_s} + \gamma \vec{B} \times \vec{\mu}_s = 0$. Here $\vec{\mu}_s$ is the spin accumulation, D_s is the spin diffusion constant, and γ is the gyromagnetic ratio. From a fit we acquire D_s and τ_s and hence we can calculate the spin relaxation length $\lambda = \sqrt{D_s \tau_s}$. For this particular dataset we find an increased $D_s = 0.052$ m^2/s compared to SiO_2, with values $\sim$0.02 m^2/s. Interestingly, $\tau_s = 390$ ps is not much different from a SiO_2-based device. The fact that it is higher than the typically observed 200 ps is due to the use of TiO_2 barriers instead of Al_2O_3, resulting in a reduced barrier roughness.[7] Note that precession measurements over 16 μm for this device yield a relaxation length of 4.5 μm, while several additional electrodes [dashed lines in Fig. 2(a)] are present between the injection and detection circuits. We obtain the same result for precession over 2 μm without any contacts in between (see Fig. 3), which indicates that the contacts do not introduce a considerable spin scattering.

For devices 1–3 the parameters obtained by fitting room temperature precession measurements are shown in Figs. 3(a)–3(c). Values for τ_s are found in the range from 50 to 480 ps for various charge-carrier densities, which is similar to what is

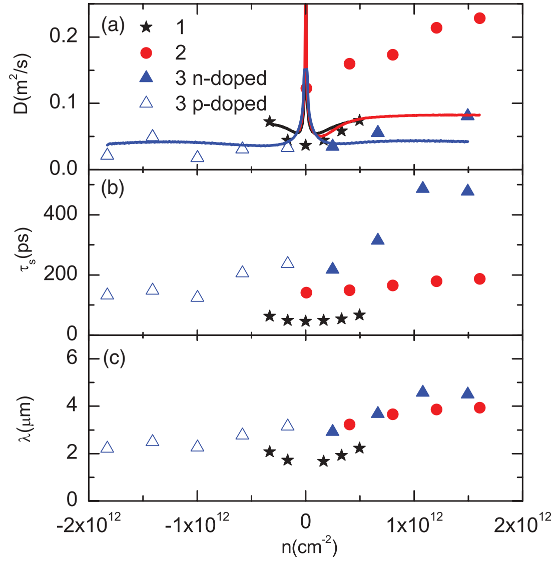

FIG. 3. (Color online) Room temperature data extracted from precession measurements for devices 1, 2, and 3 as a function of charge-carrier density, with respective injector detector spacings of 3.5, 3.5, and 2 μm. The standard fitting error lies in general within the size of data points. The barriers are made of Al_2O_3 for devices 1 and 2 and of TiO_2 for device 3. (a) Spin- and charge-diffusion constants, symbols, and lines, respectively. The latter are extracted from charge transport. (b) Spin-relaxation times. (c) Spin-relaxation lengths.

found for lower-mobility devices on SiO_2. For devices 2 and 3, D_s does not match well with the charge-diffusion constant [solid lines in Fig. 3(a)], which is obtained using the Einstein relation and charge transport measurements.[4] Because our spin relaxation length is much larger than the contact spacing the determination of D_s is less accurate[25] and therefore we use D_c to calculate λ. This way we obtain relaxation lengths up to 4.6 μm. We also measured spin transport at temperatures down to 4.2 K, which only led to a minor increase in D_s and τ_s. The behavior we measure for the p-doped part of device 3 deviates in the sense that τ_s decreases with increasing hole density. The cause for this is unclear.

In order to investigate the underlying spin relaxation mechanism in relation to the substrate and device quality, we can analyze the data from Fig. 3 in the light of the DP and EY mechanisms by looking at the relation between τ_s and τ_p. We extract the latter from charge transport measurements, using $\tau_p = \frac{2D_c}{v_F^2}$, where $v_F = 10^6$ m/s is the Fermi velocity. For DP the relation between the spin relaxation time τ_s and momentum relaxation time τ_p is given by $\frac{1}{\tau_{s,\mathrm{DP}}} = (\frac{4\Delta_{\mathrm{DP}}^2}{\hbar^2})\tau_p$, with Δ_{DP} as the effective spin-orbit coupling.[15] In Fig. 4(a) this relation is plotted for three different values of Δ_{DP}, together with the experimentally obtained data. We observe that the linear trends described by theory are not reflected by our data. On the other hand we can consider an EY mechanism, in which case the relation is given by $\tau_{s,\mathrm{EY}} = \frac{\varepsilon_F^2 \tau_p}{\Delta_{\mathrm{EY}}^2}$, where ε_F is the Fermi energy and Δ_{EY} is the spin-orbit coupling.[3,14] Figure 4(b) shows this relation for three values of Δ_{EY}. In this case the experimental data does show linear trends, but none of the sets intersect with the origin. This cannot be attributed to broadening of the density of states or finite conductivity.[9]

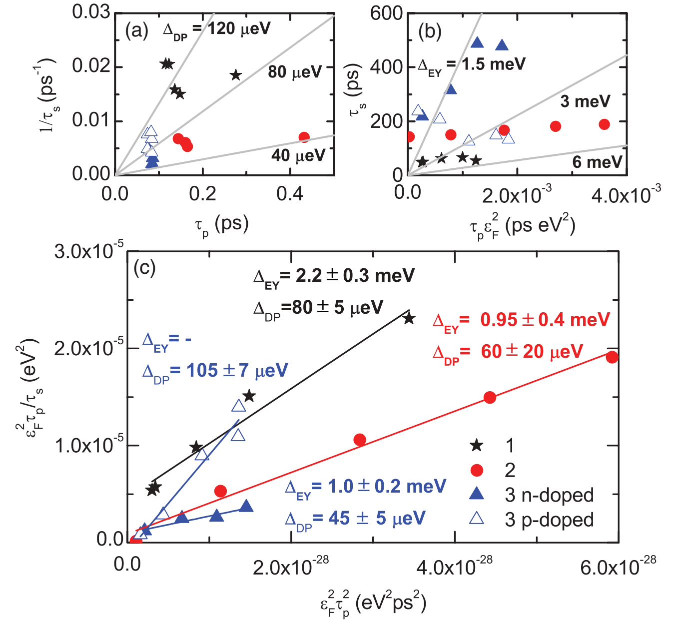

FIG. 4. (Color online) Room temperature data obtained from devices 1, 2, and 3. All error bars fall within the data point size. Linear relations allow for extraction of the spin-orbit coupling assuming (a) the DP mechanism or (b) the EY mechanism. The solid lines reflect the theoretical relation for several spin-orbit couplings. For both mechanisms the data deviates from theoretical expectations. (c) The combination of both the DP and EY mechanisms allows for extraction of the respective spin-orbit couplings using Eq. (1). The solid lines are linear fits; the error margins result from the standard error in the linear fits.

Alternatively we can consider both mechanisms simultaneously, with the overall scattering rate given by $\frac{1}{\tau_s} = \frac{1}{\tau_{s,\mathrm{EY}}} + \frac{1}{\tau_{s,\mathrm{DP}}}$, which leads to the following relation:

$$\frac{\varepsilon_F^2 \tau_p}{\tau_s} = \Delta_{\mathrm{EY}}^2 + \left(\frac{4\Delta_{\mathrm{DP}}^2}{\hbar^2}\right)\left(\varepsilon_F^2 \tau_p^2\right). \tag{1}$$

When plotting $\frac{\varepsilon_F^2 \tau_p}{\tau_s}$ versus $\varepsilon_F^2 \tau_p^2$ for our data in Fig. 4(c) we clearly observe a linear behavior for all devices. Using a linear relation we determine the slope and intersect with the y axis, which directly gives measures for both Δ_{EY} and Δ_{DP}. The deviating behavior for the p-doped side of device 3 originates from the unexpected relation between τ_s and n [Fig. 3(b)] and Δ_{EY} could not be extracted. Looking at the respective relaxation rates, we find that tuning the charge-carrier density in fact leads to very similar rates for both the DP and EY contributions. For DP we find rates in the range from 1×10^9 s^{-1} to 2×10^{10} s^{-1} and for EY from 3×10^8 s^{-1} to 4×10^{10} s^{-1}.

For comparison the analysis using Eq. (1) is applied to the room temperature spin transport data achieved for a SiO_2-based device in Ref. 4. In this case we find $\Delta_{\mathrm{DP}} \approx 90$ μeV and $\Delta_{\mathrm{EY}} \approx 2.3$ meV, which is very similar to the result for the h-BN-based devices. Likewise, the relaxation rates for both mechanisms are comparable as well, with values in the order of 10^9 s^{-1} for both mechanisms. The advantage of a h-BN-based device is that larger momentum relaxation times are achieved.

We measured spin transport in supported graphene devices at higher mobilities than achieved so far. Interestingly, we do not see an effect on τ_s, which is consistent with results that were recently achieved for SiO_2-based devices with tunable mobility.[8] The use of a h-BN substrate allowed us to exclude the influence of the SiO_2 substrate and graphene roughness on spin relaxation. These two types of graphene devices only have the contacts and the contaminants in common which therefore appear to dominate the spin relaxation properties of graphene devices. The contacts are known to have an effect,[7] but the mismatch between experimental observations and theoretical predictions is not accounted for. We observe an enhanced spin relaxation time when using TiO_2 barriers, which are smoother than Al_2O_3. The resistance of our contacts is expected to be sufficient for accurate measurement of nonlocal spin signals,[5] so the contacts are excluded as the dominant limiting factor for spin relaxation. Other factors that can be held responsible are scattering by covalently bonded adsorbates and charged impurities.[26] An interesting approach for future experiments would be to realize clean graphene flakes by removing resist residues and other contaminants. First steps have been taken by the realization of suspended graphene flakes that can be current annealed.[10] For h-BN-based devices, alternative cleaning methods, as for example, mechanical cleaning,[27] may be adopted to preserve the contacts.

In conclusion we have fabricated graphene spin transport devices based on h-BN crystals with mobilities up to 40 000 $cm^2\,V^{-1}\,s^{-1}$ that show superior spin relaxation lengths at room temperature. This is directly demonstrated by spin-valve measurements over distances up to 20 μm and confirmed by Hanle spin precession measurements, which reveal spin relaxation lengths up to 4.5 μm. The increase with respect to lower-mobility SiO_2-based devices is due to an increase in the diffusion constant; the spin relaxation time remains virtually unchanged. This is an experimental indication that the substrate and roughness are not the limiting factors for spin relaxation in graphene, which is an important observation since most research has been done on SiO_2-based devices. Other factors may be dominant, such as contaminants on the graphene flake. Concerning the relaxation mechanism, we find that our data is best described by a combination of the EY and DP mechanisms. The respective relaxation rates are found to be very similar for both mechanisms, indicating that the spin relaxation is not dominated by a single mechanism.

We acknowledge B. Wolfs, J. G. Holstein, and H. M. de Roosz for their technical assistance. This work is financially supported by the Dutch Foundation for Fundamental Research on Matter (FOM), NWO, NanoNed, and the Zernike Institute for Advanced Materials.

*p.j.zomer@rug.nl

[1] A. K. Geim and K. S. Novoselov, Nature Mater. **6**, 183 (2007).

[2] N. Tombros, C. Jozsa, M. Popinciuc, H. T. Jonkman, and B. J. van Wees, Nature (London) **448**, 571 (2007).

[3] D. Huertas-Hernando, F. Guinea, and A. Brataas, Phys. Rev. Lett. **103**, 146801 (2009).

[4] C. Józsa, T. Maassen, M. Popinciuc, P. J. Zomer, A. Veligura, H. T. Jonkman, and B. J. van Wees, Phys. Rev. B **80**, 241403 (2009).

[5] M. Popinciuc, C. Józsa, P. J. Zomer, N. Tombros, A. Veligura, H. T. Jonkman, and B. J. van Wees, Phys. Rev. B **80**, 214427 (2009).

[6] W. Han, K. McCreary, K. Pi, W. Wang, Y. Li, H. Wen, J. Chen, and R. Kawakami, J. Magn. Magn. Mater. **324**, 369 (2012).

[7] W. Han, K. Pi, K. M. McCreary, Y. Li, J. J. I. Wong, A. G. Swartz, and R. K. Kawakami, Phys. Rev. Lett. **105**, 167202 (2010).

[8] W. Han, J.-R. Chen, D. Wang, K. M. McCreary, H. Wen, A. G. Swartz, J. Shi, and R. K. Kawakami, Nano Lett. **12**, 3443 (2012).

[9] S. Jo, D.-K. Ki, D. Jeong, H.-J. Lee, and S. Kettemann, Phys. Rev. B **84**, 075453 (2011).

[10] M. H. D. Guimarães, A. Veligura, P. J. Zomer, T. Maassen, I. J. Vera-Marun, N. Tombros, and B. J. van Wees, Nano Lett. **12**, 3512 (2012).

[11] A. Avsar, T.-Y. Yang, S. Bae, J. Balakrishnan, F. Volmer, M. Jaiswal, Z. Yi, S. R. Ali, G. Guntherodt, B. H. Hong, B. Beschoten, and B. Ozyilmaz, Nano Lett. **11**, 2363 (2011).

[12] T. Maassen, J. J. van den Berg, N. IJbema, F. Fromm, T. Seyller, R. Yakimova, and B. J. van Wees, Nano Lett. **12**, 1498 (2012).

[13] T. Maassen, J. J. van den Berg, E. Huisman, H. Dijkstra, F. Fromm, T. Seyller, and B. J. van Wees, arXiv:1208.3129.

[14] H. Ochoa, A. H. Castro Neto, and F. Guinea, Phys. Rev. Lett. **108**, 206808 (2012).

[15] P. Zhang and M. W. Wu, New J. Phys. **14**, 033015 (2012).

[16] C. Ertler, S. Konschuh, M. Gmitra, and J. Fabian, Phys. Rev. B **80**, 041405 (2009).

[17] J. Martin, N. Akerman, G. Ulbricht, T. Lohmann, J. H. Smet, K. von Klitzing, and A. Yacoby, Nat. Phys. **4**, 144 (2008).

[18] B. Dlubak, M.-B. Martin, C. Deranlot, B. Servet, S. Xavier, R. Mattana, M. Sprinkle, C. Berger, W. A. D. Heer, F. Petroff, A. Anane, P. Seneor, and A. Fert, Nat. Phys. **8**, 557 (2012).

[19] K. I. Bolotin, K. J. Sikes, Z. Jiang, M. Klima, G. Fudenberg, J. Hone, P. Kim, and H. L. Stormer, Solid State Commun. **146**, 351 (2008).

[20] N. Tombros, A. Veligura, J. Junesch, J. J. van den Berg, P. J. Zomer, M. Wojtaszek, I. J. V. Marun, H. T. Jonkman, and B. J. van Wees, J. Appl. Phys. **109**, 093702 (2011).

[21] C. R. Dean, A. F. Young, I. Meric, C. Lee, L. Wang, S. Sorgenfrei, K. Watanabe, T. Taniguchi, P. Kim, K. L. Shepard, and J. Hone, Nat. Nanotechnol. **5**, 722 (2010).

[22] J. Xue, J. Sanchez-Yamagishi, D. Bulmash, P. Jacquod, A. Deshpande, K. Watanabe, T. Taniguchi, P. Jarillo-Herrero, and B. J. LeRoy, Nature Mater. **10**, 282 (2011).

[23] P. J. Zomer, S. P. Dash, N. Tombros, and B. J. van Wees, Appl. Phys. Lett. **99**, 232104 (2011).

[24] F. J. Jedema, H. B. Heersche, A. T. Filip, J. J. A. Baselmans, and B. J. van Wees, Nature (London) **416**, 713 (2002).

[25] T. Maassen, I. J. Vera-Marun, M. H. D. Guimarães, and B. J. van Wees, arXiv:1210.0093.

[26] A. H. Castro Neto and F. Guinea, Phys. Rev. Lett. **103**, 026804 (2009).

[27] A. M. Goossens, V. E. Calado, A. Barreiro, K. Watanabe, T. Taniguchi, and L. M. K. Vandersypen, Appl. Phys. Lett. **100**, 073110 (2012).